Scalable Device for Automated Microbial Electroporation in a Digital Microfluidic Platform

Andrew C. Madison,*,[†] Matthew W. Royal,[†] Frederic Vigneault,[‡] Liji Chen,[†] Peter B. Griffin,[§] Mark Horowitz,[∥,⊥] George M. Church,[‡,#] and Richard B. Fair[†]

[†]Department of Electrical and Computer Engineering, Duke University, Durham, North Carolina 27708, United States

[‡]Wyss Institute for Biologically Inspired Engineering, Boston, Massachusetts 02115, United States

[§]Stanford Genome Technology Center, Stanford University, Palo Alto, California 94304, United States
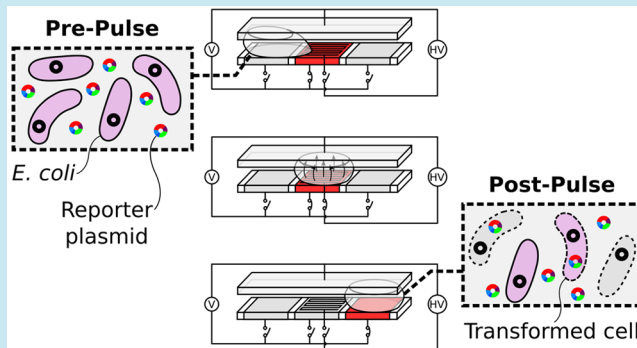
[∥]Department of Computer Science, [⊥]Department of Electrical Engineering, Stanford University, Stanford, California 94305, United States

[#]Department of Genetics, Harvard Medical School, Harvard University, Boston, Massachusetts 02115, United States

S *Supporting Information*

ABSTRACT: Electrowetting-on-dielectric (EWD) digital microfluidic laboratory-on-a-chip platforms demonstrate excellent performance in automating labor-intensive protocols. When coupled with an on-chip electroporation capability, these systems hold promise for streamlining cumbersome processes such as multiplex automated genome engineering (MAGE). We integrated a single Ti:Au electroporation electrode into an otherwise standard parallel-plate EWD geometry to enable high-efficiency transformation of *Escherichia coli* with reporter plasmid DNA in a 200 nL droplet. Test devices exhibited robust operation with more than 10 transformation experiments performed per device without cross-contamination or failure. Despite intrinsic electric-field nonuniformity present in the EP/EWD device, the peak on-chip transformation efficiency was measured to be $8.6 \pm 1.0 \times 10^8$ cfu·μg^{-1} for an average applied electric field strength of 2.25 ± 0.50 kV·mm^{-1}. Cell survival and transformation fractions at this electroporation pulse strength were found to be 1.5 ± 0.3 and $2.3 \pm 0.1\%$, respectively. Our work expands the EWD toolkit to include on-chip microbial electroporation and opens the possibility of scaling advanced genome engineering methods, like MAGE, into the submicroliter regime.

KEYWORDS: *digital microfluidics, electroporation, transformation, droplet*

Automation and miniaturization of gene delivery methods hold the promise of revolutionizing synthetic biology. Such advances may fundamentally alter our approach to human health, security, and manufacturing, but current protocols rely on cumbersome experimental systems that limit the rate of biological construct development. Microfluidics-based gene transfer technologies overcome these barriers through the development of devices that couple scalable fluid handling and gene transfer capabilities,[1,2] yet few microfluidics gene transfer technologies have been adopted by the biological research community. To address this technological gap, we refine conventional bulk electroporation into an electrowetting-on-dielectric (EWD) digital microfluidic (DMF) format, enabling the characterization of high-efficiency microbial transformation in a programmable, submicroliter droplet-based workflow for the first time. The present work describes microbial survival, molecular transport, and transformation rates associated with an electroporation (EP) device that scales with the geometry of a coupled EWD DMF actuator. Building on our previous work,

our results suggest that EWD DMF is a viable approach to realizing microbial EP in EWD actuators of arbitrary size.[3,4]

Many strategies have emerged as a means of automating and miniaturizing gene transfer, but the process remains, to a great extent, uncharacterized for EWD systems. Current literature demonstrates a variety of EP electrode geometries, including parallel plate electrodes,[5−12] coplanar electrodes,[13−26] and three-dimensional microstructures fabricated into channel side walls[27−33] as well as more exotic approaches that exploit nanostructure for local electric field enhancement.[7,11,26,34] Recent efforts have demonstrated microbial electroporation in a range of fluidic formats as well. Static microwell,[16,17,22,23,35] continuous,[5−9,11,12,21,24−27,30,31,36−39] and discrete[20,33,40,41] droplet-based pressure driven flow formats as well as hydrodynamic formats that utilize dielectrophoresis,[13,18,19] flow-focusing,[10] and vortex-assisted[42] approaches have been
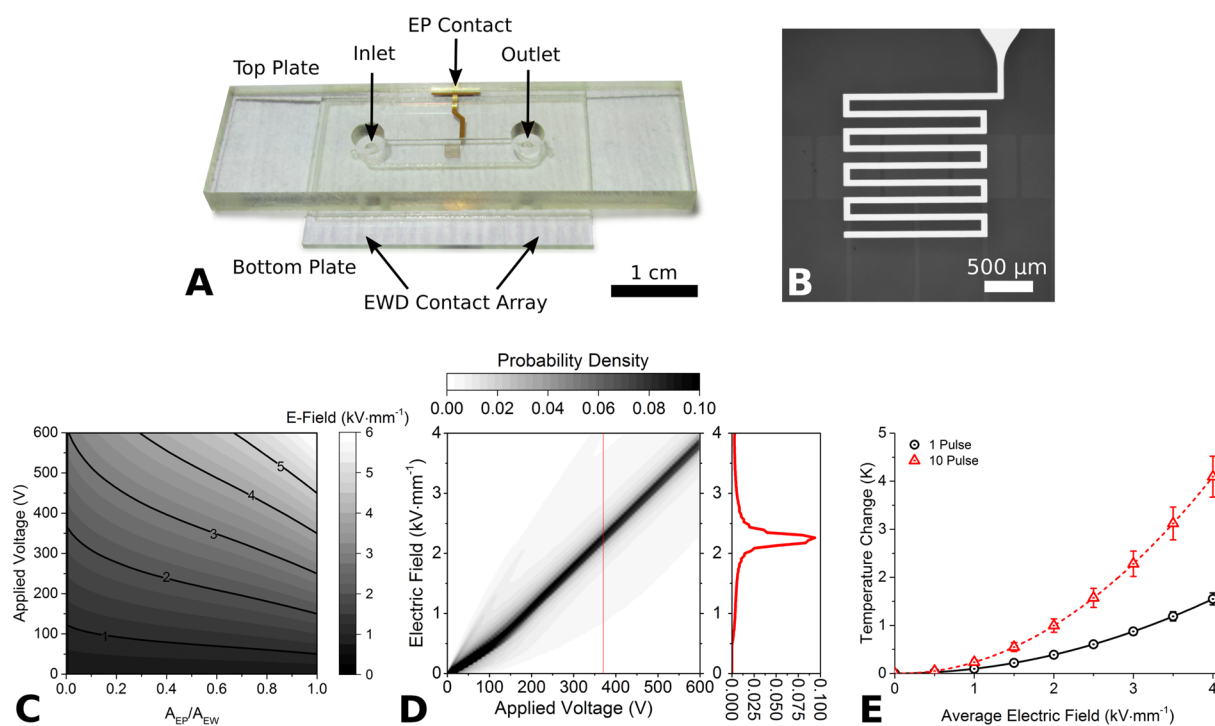
Figure 1. (A) Photograph of the complete EP/EWD device assembly. (B) Micrograph of the integrated EP/EWD device. (C) Average electric field strength within a 200 nL droplet region plotted as a contour surface for the fraction of EP coverage, A_{EP}/A_{EWD}, and applied EP bias. (D) Contours of the probability density of the computed electric field strength resulting from a range of EP biases applied to the EP electrode. The profile plot (right) shows the distribution of the electric field at an optimum EP bias for electroporation in single pulse experiments, 370 V. The profile plot reflects an average field of 2.25 ± 0.50 kV·mm^{-1}. (E) Estimated temperature change for single (circles) and 10-fold (triangles) pulses assuming a 5× increase in solution conductivity due to bacterial permeabilization during electroporation.

implemented as fluid handling strategies in microelectroporation devices. The wide assortment of microfluidic and electrostatic capabilities is a testament to the demand for scalable and automatable electroporation microsystems, which highlights the importance of matching the fluid handling technique with an appropriate electrode configuration.

The versatility and scalability of the EWD DMF toolkit suggest that the technology is poised to make a deep impact in the growing industry of genome engineering research.[43−49] EWD involves modulation of the wetting behavior of a polarizable liquid droplet on a hydrophobic, insulated electrode through the application of an electric field and has been proven for the manipulation of biological samples.[46,50−55] In 2014, Illumina, Inc. unveiled a library preparation tool that uses EWD DMF for the automated preparation of libraries for whole-genome and whole-transcriptome sequencing.[56] Similarly, EWD DMF has been commercialized by Genmark Diagnostics, Inc. for completely automated and multiplexed nucleic acid extraction, amplification, and detection.[57] Moreover, Shih et al. recently highlighted the utility of DMF for automating gene assembly through the demonstration of a hybrid discrete flow microfluidics platform that leveraged EWD to assemble plasmid constructs and a pressure-driven stage to expose droplets of an *Escherichia coli* suspension to EP fields.[39] Although striking in their execution of scaled combinatorial DNA assembly and microbial transformation, their hybrid platform did not integrate electroporation into the droplet-based format native to EWD DMF, which underscores the need for an integrated EP/EWD solution. While our past work focused on proof-of-concept demonstrations of EP in EWD devices, it failed to

include characterization of on-chip transformation rates with respect to EP pulse configurations.[3,4]

The present work addresses the technological gap of EWD-based microbial transformation through the characterization of a device capable of supporting discrete fluid transport and robust electroporation of microbial cells in a submicroliter droplet. The integration of EP functionality into a format compatible with EWD is motivated by the concept of embedding an additional metallic structure into an otherwise conventional parallel plate EWD platform. This article extends our previous work, which outlines a proof-of-concept for EP and droplet transport in partially shielded EWD devices.[3,58]

■ EXPERIMENTAL METHODS

The primary objective of our experimental approach involves the characterization of an EP/EWD device with respect to cell survival, plasmid transport, and transformation efficiency for a range of EP pulse strengths and pulse numbers. As shown in Figure 1A,B, a meandering electrode patterned on the EWD dielectric was chosen as a prototype EP device geometry. Common EWD microfabrication methods were employed for the batch production of the EP/EWD devices.[58,59] As previously outlined for bench-scale MAGE, our experimental procedure followed six steps for the EWD-enabled transformation of *E. coli* cells: cell growth, media exchange, electroporation, cell recovery, sample dilution, and quantification of survival and transformation rates.[1]

Cell Growth and Media Exchange. The EcNR2 *E. coli* strain used in this study is resistant to chloramphenicol, protecting against contamination during sample preparation and storage.[1] Liquid cultures of the EcNR2 strain (Addgene no.
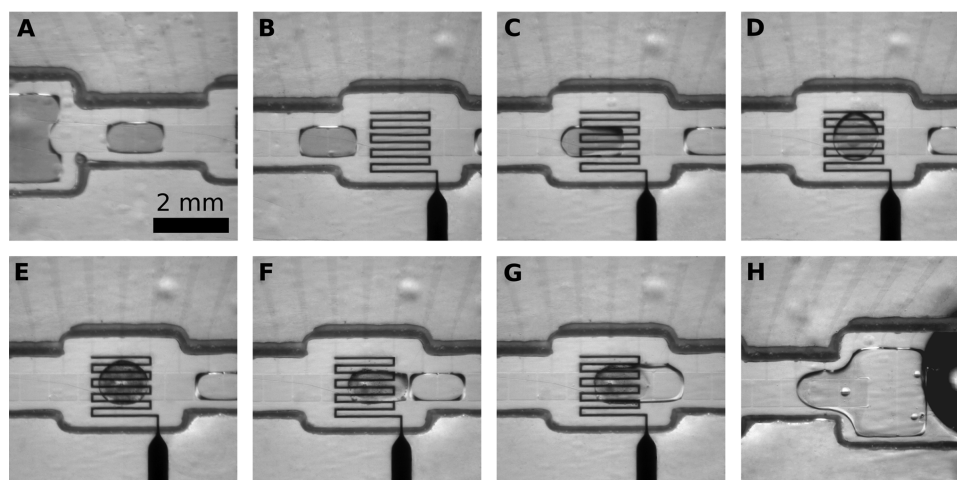
Figure 2. EWD-enabled transformation of 200 nL droplets containing *E. coli* and *pGERC*. (A−C) A single 2× (200 nL) aqueous droplet containing *E. coli* and *pGERC* is dispensed from the inlet reservoir and transported to the EP/EWD electrode in preparation for EP pulse delivery. (D−E) EP pulses of various strength (0−3 kV·mm^{-1}), number (1 or 10), and shape (exponential decay or trapezoidal) were administered to the droplet before (F−H) the droplet is merged with a 200 nL recovery droplet and actuated to the outlet reservoir, where the entire content of the outlet reservoir was then collected.

26931) were obtained and immediately streaked onto Luria Broth (LB) (Affymetrix, Inc.) agar plates containing 12.5 μg·mL^{-1} chloramphenicol (Teknova, Inc.) and stored at 4 °C. As outlined in the Supporting Information, common procedure for the production of electrocompetent *E. coli* cultures was followed.[1,2]

Aliquots of 1 mL of mid-log-phase cultures were washed twice with ice-cold 0.01% (v/v) Tween 20 in nuclease-free DI water and resuspended in 200 μL of ice-cold 0.05% (v/v) Tween 20 in nuclease-free DI water, resulting in an electrocompetent cell concentration of $2.67 \pm 1.2 \times 10^9$ cells·mL^{-1}. To this suspension was added 5 μL of 77.0 ± 7.1 ng·μL^{-1} *pGERC* reporter plasmid DNA (Addgene plasmid no. 47441), resulting in a final DNA concentration of 1.88 ± 0.03 ng·μL^{-1}.[60] The *pGERC* plasmid carries a gene that encodes resistance to kanamycin, an antibiotic that inhibits protein synthesis in nonresistant bacteria.[61,62] As outlined in the Supporting Information, the conductivity of the cell/DNA suspension was measured to be $4.14 \pm 0.38 \times 10^{-2}$ μS·cm^{-1}.

EP/EWD Device Design. The EP/EWD device design included an EWD electrode length of 700 μm and an EP wire width of 60 μm, which shielded 34% of the EWD electrode area. A fully assembled EP/EWD device and a photomicrograph of the EP electrode are shown in Figure 1, panels A and B, respectively. The bottom plate comprised 22 EWD electrodes that make up two 3.5 × 2.1 mm reservoirs and a single lane of sixteen 700 × 700 μm channel electrodes, spaced with a 15 μm interelectrode gap, a 2 μm thick SU-8 EW dielectric, a 20 nm SiO$_2$ adhesion layer, a single Ti:Au (5:200 nm) EP electrode, a 174 ± 3 μm Duralar polyester gasket, and a 70 ± 10 nm film of Cytop hydrophobic coating. The meandering EP electrode is 60 μm wide and shields 34% of the underlying EWD electrode from a centered droplet.

As summarized in the Supporting Information, a coupled quasi-static finite element model (FEM) of electric potential and temperature profiles in the EP/EWD device was developed using Comsol Multiphysics to estimate the probability density of intradroplet electric field strengths and temperature changes in the device during single and multiple pulse experiments for the experimental range of EP biases. Profilometry traces of the

EWD gasket walls near the EP/EWD and voltages measured during EP pulse delivery informed the simulation geometries and boundary conditions. The family of solutions of the average electric field strength within a 200 nL droplet region is plotted as a contour surface for the fraction of EP coverage, A_{EP}/A_{EWD}, and applied EP bias in Figure 1C. Figure 1D shows contours of electric field distributions computed for a 200 nL droplet centered over an EP/EWD device with a fraction of EP coverage of 0.34. Anticipated temperature responses for single and ten pulse EP schemes is shown in Figure 1E. As summarized in the Supporting Information, our calculation of Joule heating within the EP/EWD assumes a 5× increase in electrical conductivity due to microbial permeabilization during electroporation pulse delivery.[63−66]

EP/EWD Chip Staging. Individual EP/EWD devices were loaded into a test jig and secured in place by stage-mounted slide clips as shown in Figure S6. A CCD camera (model avA1000-120kc, Basler) and telephoto lens (Optem Zoom 125, Qioptik) mounted beneath the EWD stage allowed real-time microscopic image capture of each experiment. Electrical connections to the bottom and top plates were made by attaching a ribbon connector to the EWD test clip and the EP/EWD ground clip to the lateral side of the top plate.[58] Alligator clips were used to connect the EP (+) electrode contact and the EP/EWD ground to the positive and negative terminals of the MicroPulser electroporator unit (Bio-Rad Laboratories, Inc.), respectively.

Once the electrical connections were established, ~25 μL of 2 cSt silicone oil (Advanced Liquid Logic, Inc.) was added to the EWD device via the pipet inlets. The EW voltage was set to a 1 kHz, 50 V$_{p-p}$ sine wave, and a custom EWD graphical user interface[59] (GUI) (available upon request) was used to energize all four EWD reservoir electrodes in the reservoir on one side of the EP/EWD device. With the EWD reservoir electrodes activated, 2 μL of the EcNR2 cells and DNA mixture was pipetted into one EWD reservoir. Then, 2 μL of recovery media, which consisted of LB containing 0.05% (v/v) Tween 20, was pipetted into the second EWD reservoir.

On-Chip Transformation. A simple EWD protocol was developed for the demonstration of on-chip EP in the EWD
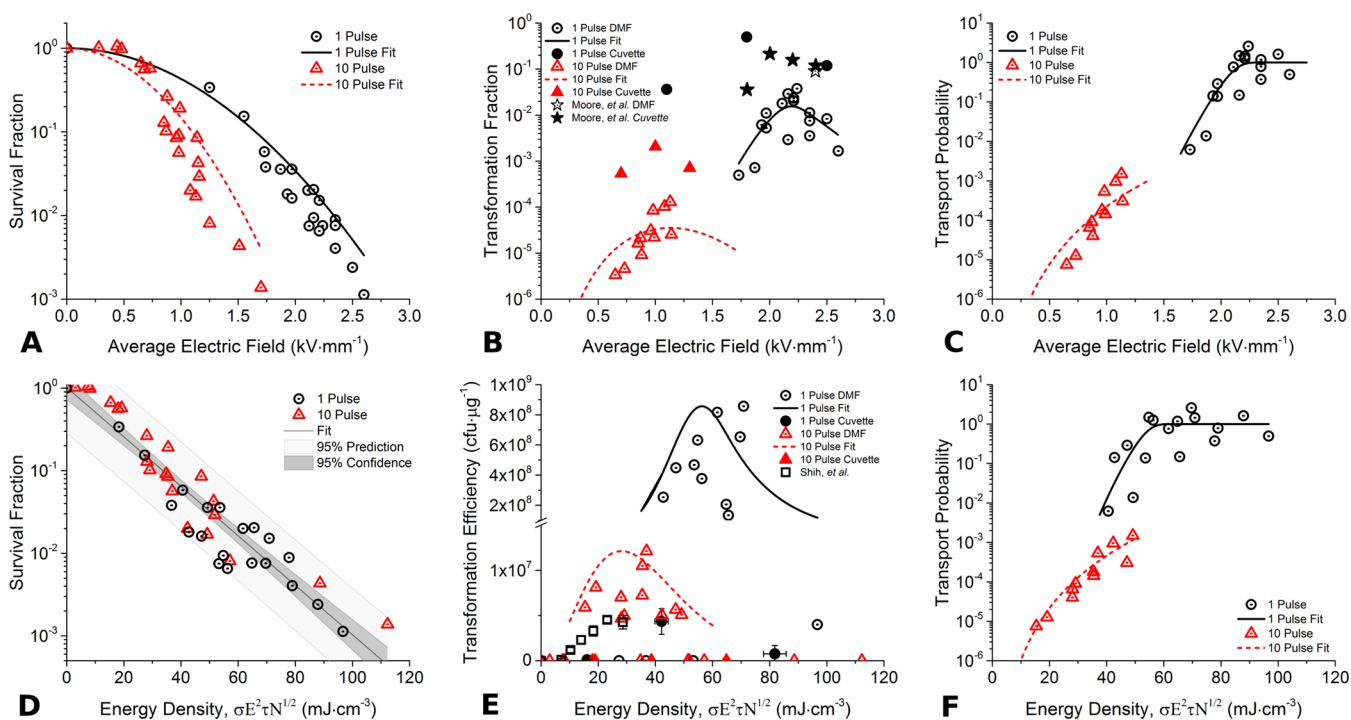
Figure 3. Cell survival, transformation, and plasmid transport observed in the EP/EWD device for a single pulse (circles) and ten pulses (triangles). Cell survival fraction (A), transformation fraction (B), and transport probability (C) plotted with respect to average intradroplet electric field strength. Cell survival fraction (D), transformation efficiency (E), and transport probability (F) plotted with respect to pulse scheme energy density ($\sigma E^2 \tau N^{1/2}$). For direct comparison to recent work regarding the electroporation of *E. coli*, transformation fractions and efficiencies reported in cuvette (solid) and microfluidic (hollow) systems are included in (B) and (E).

environment. The on-chip protocol is summarized in Figure 2. With the EWD reservoirs loaded with the EcNR2 culture/DNA mixture on one side of the EP/EWD chip and the recovery media in the opposing reservoir, the EWD control GUI was used to dispense and transport a 2× (200 nL) droplet of recovery media to an EWD electrode adjacent to the site of the EP/EWD device.

Once the recovery droplet was in place, a 2× (200 nL) droplet of cells/DNA was transported to the EP/EWD device, as shown in Figure 2A–D. With the cell/DNA droplet positioned over the EP/EWD electrode, EP pulses of variable strength and number were administered to the droplet. Figure 2D,E shows the droplet before and after the delivery of a single EP pulse. The actual voltage applied between the EP (+) terminal and the EP/EWD ground was measured with an oscilloscope (model 54624A, Agilent Technologies) and a 1:100 probe. We used the electrostatic FEM to estimate the average electric field strength inside of the droplets using knowledge of the gasket geometries and the EP biases measured during pulse delivery. As shown in Figure 2F,G, the recovery droplet was actuated to the EP/EWD device immediately after the EP pulse to rescue the porated cells and facilitate droplet removal from the device.

Once the cell/DNA and recovery media droplets were mixed, the resulting 4× droplet was actuated to the recovery reservoir for collection as shown in Figure 2G–H. The entire content of the recovery reservoir as well as additional silicone oil, which totaled 5 µL, was collected. The collected fluid, 2.4 µL of which was aqueous, was added to 1 mL of LB in 15 mL plastic cell culture tubes prewarmed to 30 °C. Collection was noted, and the tubes were incubated with agitation at 30 °C for 2.5 h.

This protocol was repeated for a range of EP pulses that varied in average strength from 0 to 3 kV·mm^{-1} (0−600 V) for single decaying eponential pulses with a time constant, τ, of 6.0 ± 0.1 ms and for ten trapezoidal pulses of width 3.0 ± 0.0 ms. [A simple CMOS circuit was used for rapid delivery of ten EP pulses.[59]] Obvious anomalous behaviors associated with the pulse delivery and postpulse appearance of the EP/EWD chip were noted. The EP/EWD chips were reused for multiple experiments but were flushed with silicone oil between pulses. To test for cross-contamination, 2× droplets of LB were actuated through freshly flushed devices and cultured. Zero growth was observed after 2.5 h of recovery and plating on LB agar containing 12.5 µg·mL^{-1} chloramphenicol, indicating the reusability of the devices.

Off-Chip Sample Processing. Common cell recovery, dilution, growth, and quantification methods were employed to determine survival and transformation rates for each EP experiment.[1−3] Cell recovery was conducted at 30 °C for 2.5 h with agitation. Serial dilution of recovered samples was carried out to factors of 10^{-1}, 10^{-2}, 10^{-3}, and 10^{-4}.

Experimental controls were established by plating 50 µL of the 10^{-3} and 10^{-4} dilutions on separate halves of LB agar plates containing 12.5 µg·mL^{-1} chloramphenicol (cat. no. L1013, Teknova, Inc.). An experimental group was established by plating 50 µL of the original sample and the 10^{-1} dilution on separate halves of LB agar plates that contained 12.5 µg·mL^{-1} chloramphenicol and 50 µg·mL^{-1} kanamycin (cat. no. L1257, Teknova, Inc.). Both groups of plates were then incubated at 30 °C for 18 h.

Photographs were taken of all plates using a standard compact digital camera (PowerShot A2300 HD, Canon Inc.), and resulting colonies were counted manually using the Cell

Counter plugin in the image processing suite ImageJ (National Institutes of Health, USA). Survivors (S) were counted as the number of colonies that grew on the LB–chloramphenicol control plates, and transformants (T) were counted as the number of colonies that grew on the LB plates that contained chloramphenicol and kanamycin. Colony counts for each plate were adjusted for their respective dilutions.

The statistical model offered by Canatella and Prausnitz was adopted for characterizing the fraction of cells that survived, received at least one copy of the plasmid, and was transformed by the EP pulse.[67] As shown in eq 1, the survival fraction, S_f, of each sample in the control group was defined as the ratio of survivors to the number of survivors determined for droplets that were not pulsed, S_0. Hence, each group contained a control sample that was actuated in the EP/EWD device but not exposed to an EP pulse. The transformation fraction, T_f, of each sample in the experimental group was defined as either the ratio of transformants to the number of survivors that were counted for corresponding samples in the control group or the product of the survival fraction and the likelihood of plasmid transport, N_f, as shown in eq 2. Trends in survival, plasmid transport, and transformation were investigated as functions of average electric field strength and energy density through the application of this simple model.

$$S_f = \frac{S}{S_0} = e^{-\alpha\|\bar{\mathbf{E}}\|^2} \tag{1}$$

$$T_f = \frac{T}{S} = S_f N_f = e^{-\alpha\|\bar{\mathbf{E}}\|^2}(1 - e^{-\beta\|\bar{\mathbf{E}}\|^\delta}) \tag{2}$$

Cuvette-Based Transformation. To contextualize on-chip results, the transformation procedure described above was also execued in standard 0.1 cm EP cuvettes (no. 1652089, Bio-Rad Laboratories, Inc.). A *pGERC* reporter plasmid concentration of 1.53 ± 0.10 ng·μL^{-1} was present during the cuvette-based EP of EcNR2 suspensions that ranged in volume from 50 to 100 μL per cuvette. Exponentially decaying EP pulses of strengths 0.0, 1.1, 1.8, and 2.5 kV·mm^{-1} ($\tau = 5.5 \pm 0.2$ ms) were applied as single pulses in one set of trials and with strengths of 0.0, 0.7, 1.0, and 1.3 kV·mm^{-1} ($\tau = 5.1 \pm 0.1$ ms) for ten pulses in a second set. Recovery was initiated in the EP cuvettes with 1 mL of LB, and the suspension was immediately transferred to growth tubes for a 2 h incubation with agitation at 30 °C. Recovered suspensions were then diluted by factors of 10^{-4} and 10^{-1} for plating on control and selection plates, which contained 12.5 μg·mL^{-1} chloramphenicol and 12.5 μg·mL^{-1} chloramphenicol plus 50 μg·mL^{-1} kanamycin, respectively. All samples were plated with a volume of 50 μL. Resulting colonies were counted and anaylzed as previously described.

■ RESULTS AND DISCUSSION

On-chip, EWD-based EP was successfully demonstrated. A total of 6 EP/EWD chips were used in 44 individual, on-chip EP experiments. The EP/EWD chips were found to be reusable, robust, resistant to contamination from previous experiments, and able to withstand hundreds of EP pulses with minimal signs of dielectric breakdown or fluidic failure.

Cell Survival. Cell survival decreased exponentially as the average electric field strength and energy density of the EP pulses increased. Figure 3A shows a semilog plot of the survival fraction measured for the electroporation of EcNR2 cells in the EP/EWD device for one (circles) and ten (triangles) EP pulses ranging in average electric field strength from 0 to 2.6 kV·

mm^{-1}. The ten-pulse EP/EWD protocol exhibited significantly higher lethality than the single-pulse EP/EWD protocol, which is likely an effect of excessive electropore accumulation as well as Joule heating, as predicted in the thermal analysis summarized in Figure 1E. Curve fits are shown to illustrate the general trends observed for one (solid line) and ten (dotted line) EP pulses. The decay constant, α, for the single and ten-pulse curve fits according to eq 1 were determined to be 0.843 ± 0.028 and 1.91 ± 0.22 mm^2·kV^{-2}, respectively. As shown in Figure 3D, survival fraction trends for the one and ten pulse experiments collapsed to a single trendline when plotted against the product of pulse energy density and the square root of the number of pulses ($\sigma\tau E^2 N^{1/2}$). Linear regression was used to determine the slope and intercept of this relationship, which were found to be -0.0300 ± 0.001 cm^3·mJ^{-1} and 0.009 ± 0.074, respectively ($R^2 = 0.91$).

Transformation. The transformation of EcNR2 cells in the EP/EWD device exhibited global optima that depended heavily on the average electric field strength and pulse number. As shown in Figure 3B,E, the transformation fraction observed for single pulse trials peaked at 3.8% (8.56×10^8 cfu·μg^{-1}) for an electric field strength and energy density of 2.25 kV·mm^{-1} and 70.9 mJ·cm^{-3}, respectively. The single pulse peak transformation field strength of 2.25 kV·mm^{-1} represents a 25% increase in the reported optimum field strength of 1.8 kV·mm^{-1} for a standard EP cuvette.[1,68] In contrast, the transformation fraction observed for experiments that utilized ten pulses peaked at 0.013% (1.21×10^7 cfu·μg^{-1}) for an average electric field strength and energy density of 1.18 kV·mm^{-1} and 36.9 mJ·cm^{-3}, respectively.

Differences in optimum average EP field strengths between the on-chip and standard cuvette formats are likely the result of a nonuniform electric field profile produced by the EP/EWD device. EP field nonuniformity that results from the nonplanar EP electrode geometry reduces the efficiency of the applied field to porate exposed cells during pulse delivery. As shown in Figure S2, electric field profiles include regions of low field strength near regions of the EWD dielectric that are uneclipsed by the EP electrode. Hence, a higher average field strength is required to compensate for these regions of low field strength.

In terms of transformation efficiency, the EP/EWD device outperformed comparable cuvette-based trials as well as recent on-chip results reported elsewhere.[39] Figure 3E shows peak transformation efficiencies for single pulse experiments in EP/EWD transformed *E. coli* that are in excess of 15 times more efficient than our most efficient cuvette-based control (solid circles) and recent on-chip EP results (hollow squares) reported by Shih et al.[39] Although this effect is due in part to differences in the concentration of DNA used in each study, it reveals that the transformation efficiency in the EP/EWD device is comparable to that of standard bench-scale methods and recent advancements of droplet-based EP. Despite the high transformation efficiency observed in the EP/EWD device, fractional transformation observed in the device did not compare as well to comparable trials executed in standard EP cuvettes and on a recently reported commercial DMF platform.[4] As shown in Figure 3B, cuvette-based transformation for both the single (solid circles) and ten (solid triangles) pulse experiments from the present work as well as single pulse experiments reported by Moore et al. (stars) consistently yielded transformation fractions 1 order of magnitude greater than the EP/EWD device presented in this work (hollow circles and hollow triangles).[4] This disparity may be explained as a

Table 1. Comparison of Recent Microfluidic Platforms for Microbial Electroporation

parameter	unit	microfluidics platforms for electroporation			
		Shih et al.[39]	Moore et al.[4]	Garcia et al.[64]	this work
type of microfluidics		DMF, droplets in channel	DMF	continuous flow	DMF
dispensing volume	μL	0.2	0.35	500[a]	0.2
microbe strain		E. coli DH5α	E. coli EcNR2	E. coli K12 WT	E. coli EcNR2
DNA construct		multiple plasmids	oligonucleotide	plasmid	plasmid
DNA construct size	kb	3	0.09	3	5
pulse field strength	kV·mm^{-1}	0.18	2.4	1.25	2.25
exposure time	ms	100	6	5	6, 3
pulse shape		trapezoidal	exp. decay	triangular	exp. decay, trapezoidal
number of pulses		3	2, rev. polarity	1	1, 10
peak efficiency	cfu·μg^{-1}	4.5×10^6	9.0%[b]	4.0×10^7	8.6×10^8

[a]Flow rate reported as 500 μL·min^{-1}. [b]Transformation fraction reported.

result of EP field nonuniformity and moderate Joule heating on the order of a few degrees, as predicted in the Joule heating analysis summarized in Figure 1E.

Plasmid Transport. The fraction of cells that received a copy of the plasmid was computed as the quotient of the transformed colony count and the survival cell trend. As shown in Figure 3C,F, the transport probability for single pulse EP/EWD experiments asymptoted to unity near an average electric field strength of 2.25 kV·mm^{-1}. Transport probabilities for the ten-pulse experiments peaked at 0.02, which occurred around 1.13 kV·mm^{-1} and 50 mJ·cm^{-3}. The discrepancy in performance between the single and ten pulse experiments can likely be attributed to the exponential proportionality between the electric field strength and electropore population for a given cell.[69,70]

Nonideal Device Behavior. Several instances of nonideal behavior were observed. Failure mechanisms observed for the EP/EWD device included electryolysis of the aqueous droplet during the EP pulse, postpulse contact line pinning, EW dielectric charging and breakdown, and top plate breakdown. Droplet electrolysis was by far the most commonly observed fault, occurring in all EP experiments with EP pulses greater than ∼0.75 kV·mm^{-1} in average strength. Postpulse contact line pinning and top plate breakdown were also observed, but they were not as frequent as droplet hydrolysis. The application of a single 2.25 ± 0.50 kV·mm^{-1} EP pulse was capable of producing a distribution of bubbles inside of the pulsed droplet. This effect was found to occur more frequently and more intensely at higher electric field strengths.

The effect of electrolysis on cell survival, plasmid transport, and transformation in the EP/EWD device reported here remains unclear. However, localized pH variations caused by the electrolysis of water and subsequent ion flux near EP electrodes are known to degrade cell survival in EP protocols.[71−73]

In addition to hydrolysis, EP pulses were found to occasionally cause contact line pinning near edges of the device layer. Following the delivery of an EP pulse of sufficient strength, in several instances cell/DNA droplets were slow to actuate away from the EP/EWD device or were pinned to the EP device. In cases where postpulse contact line pinning was observed, merging the recovery droplet with the pulsed droplet aided in droplet removal. Even after such an occurrence, the EP/EWD devices were typically able to be reused for multiple subsequent transformation experiments. The cause of postpulse contact line pinning could be due to several possibilities, including dielectric breakdown, deformation of the hydro-

phobic layer, or changes in the physicochemical properties of the aqueous droplet. Although the precise mechanisms of the nonideal device behavior remain uncharacterized, our work identifies droplet electrolysis and contact line pinning as primary targets of optimization for future iterations of the EP/EWD device.

Performance Comparison. In terms of volume scaling and peak efficiency, the performance of the EP/EWD device compares favorably against recent reports of microfluidics-enabled microbial transformation platforms, which included DMF,[4] discrete,[39] and continuous[64] flow formats. Table 1 summarizes the performance of several recent microfluidic platforms including the EP/EWD device reported in the present work.

Our EP/EWD device was matched in volume-scaled operation at 200 nL in the DMF/discrete-flow hybrid device reported by Shih et al.[39] The reduction of droplet size is important for future efforts that aim to process many droplets in massively parallelized assays on DMF platforms of manageable size. Thus, the demonstration of EP in microfluidics platforms that scale well into the picoliter regime is an essential milestone in the path toward automating advanced genome engineering methods.

One drawback of volume-scaled EP/EWD is the intrinsically reduced yield associated with transformation in reduced fluid volumes. To match the yield of the continuous flow platform reported by Garcia et al., which continuously produced transformants at rates approaching 1×10^{11} cfu·$(\mu$g·h)$^{-1}$, our EP/EWD device would have to process 100 droplets per hour with a transformation efficency approaching 1×10^9 cfu·μg^{-1}.[64] Although matching such a high yield with a single EP/EWD device would be an arduous task in its current form, parallel device operation could offer comparable performance to the continuous flow strategy with the additional benefits of it being a reconfigurable, pumpless, and software-driven fluidic system.

With the exception of the 350 nL proof-of-concept EP/EWD work offered by Moore et al., the scaled EP/EWD device surpassed other recent devices in terms of peak transformation efficiency.[4] The EP/EWD device reported herein was nearly 20 and 200 times more efficient than devices reported by Garcia et al. and Shih et al., respectively.[39,64] The capability of the EP/EWD device to transform cells with efficiencies exceeding those of devices in which uniform fields were used underscores the flexibility of EP in terms of field nonuniformity. Although much work remains in the optimzation of each technological approach, the positive results observed with the EP/EWD device along with the benefits of programmatic and

reconfigurable operation of DMF, in general, give promise to the application of EWD DMF to the challenge of scaling and automating complex genome engineering methods for the lab-on-a-chip (LoC) environment.

CONCLUSIONS

The integration of an EP device layer into an EWD digital microfluidic LoC environment is a response to the increasing demand from the synthetic biology community for instrumentation capable of handling a multitude of volume-scaled gene transfer experiments in parallel and under programmatic control. Our work demonstrates an effective EP/EWD device and characterizes its performance in terms of cell survival, plasmid transport, and transformation rates with respect to average electric field strength, energy, and pulse number. The proposed meandering electrode design proved capable of exposing droplets of *E. coli* to tunable EP fields of sufficient strength to drive transformation at efficiencies comparable to those of benchtop EP cuvettes while minimally impacting electrowetting-driven droplet transport.

Advancement of EWD-enabled microbial transformation will drive the development of next-generation platforms and facilitate the use of labor-intensive genome editing protocols that rely on iterative and parallel processes. Demonstrations of high-performance on-chip cell growth, media exchange, recovery, and selection remain unreported, but they must be addressed to enable fully automated multicycle operation. Improvements in the transformation efficiency must also be investigated to identify optimal electrode designs and EP pulse parameters. Additionally, the use of pH buffering agents in the droplets and active cooling elements coupled to the EP/EWD chip are two strategies that may mitigate the extensive cell death observed in multiple pulse experiments.

A mature EP/EWD capability would profoundly impact the field of synthetic biology by accelerating the pace of automated genome engineering and expanding the reach of current experimental protocols to simultaneously handle many droplet-based genome modification experiments. Future implementations of the EP/EWD approach will deliver next-generation automated genome engineering methods, like volume-scaled MAGE or droplet-based cell-free expression systems, that may revolutionize biomaterial development and discovery.

ASSOCIATED CONTENT

ⓢ Supporting Information

The Supporting Information is available free of charge on the ACS Publications website at DOI: 10.1021/acssynbio.7b00007.

Device layout, coupled electrostatic/Joule heating analysis, microfabrication, synthetic gene construct, cell suspension preparation, media exchange, and EP/EWD chip staging (PDF)

AUTHOR INFORMATION

Corresponding Author

*Phone: +1 (704) 682 8825. E-mail: andrew.c.madison@ieee.org.

ORCID

Andrew C. Madison: 0000-0002-9456-2754
Frederic Vigneault: 0000-0002-9163-1558
Mark Horowitz: 0000-0003-3245-7542
George M. Church: 0000-0003-3535-2076

Author Contributions

A.C.M. designed, simulated, and fabricated devices, executed experiments, and wrote the manuscript. M.W.R designed, simulated, and fabricated devices and aided in experiment design and execution. F.V. designed and conducted experiments and synthesized reporter plasmid DNA. L.C. aided in experiment execution. P.B.G., M.H., G.M.C., and R.B.F. designed experiments, provided scientific guidance, and managed project funding.

Notes

The authors declare no competing financial interest.

ABBREVIATIONS

DMF, digital microfluidic; DNA, deoxyribonucleic acid; EcNR2, *E. coli* strain; EP, electroporation; EWD, electrowetting on dielectric; FEM, finite element model; GUI, graphical user interface; LB, luria broth; LoC, lab on a chip; MAGE, multiplex automated genome engineering; pGERC, reporter plasmid DNA; SU-8, epoxy-based negative resist

REFERENCES

(1) Wang, H. H., Isaacs, F. J., Carr, P. A., Sun, Z. Z., Xu, G., Forest, C. R., and Church, G. M. (2009) Programming cells by multiplex genome engineering and accelerated evolution. *Nature* 460, 894−898.

(2) Isaacs, F. J., et al. (2011) Precise Manipulation of Chromosomes *in vivo* Enables Genome-Wide Codon Replacement. *Science* 333, 348−353.

(3) Sandhal, M., Punnamaraju, S., Madison, A. C., Harrington, J., Royal, M. W., Fair, R. B., Eckhardt, A., Sudarsan, A., and Pollack, M. (2013) Software Automated Genomic Engineering (SAGE) Enabled by Electrowetting-on-Dielectric Digital Microfluidics, *Proceedings of the 17th International Conference on Miniaturized Systems for Chemistry and Life Sciences*, pp 1260−1263, Piccadilly, London.

(4) Moore, J. A., Nemat-Gorgani, M., Madison, A. C., Sandahl, M. A., Punnamaraju, S., Eckhardt, A. E., Pollack, M. G., Vigneault, F., Church, G. M., Fair, R. B., Horowitz, M. A., and Griffin, P. B. (2017) Automated electrotransformation of Escherichia coli on a digital microfluidic platform using bioactivated magnetic beads. *Biomicrofluidics* 11, 014110.

(5) Lu, H., Schmidt, M. A., and Jensen, K. F. (2005) A microfluidic electroporation device for cell lysis. *Lab Chip* 5, 23−29.

(6) Yamauchi, F., Kato, K., and Iwata, H. (2005) Layer-by-Layer Assembly of Poly(ethyleneimine) and Plasmid DNA onto Transparent Indium-Tin Oxide Electrodes for Temporally and Spatially Specific Gene Transfer. *Langmuir* 21, 8360−8367.

(7) Miyano, N., Inoue, Y., Teramura, Y., Fujii, K., Tsumori, F., Iwata, H., and Kotera, H. (2008) Gene transfer device utilizing micron-spiked electrodes produced by the self-organization phenomenon of Fe-alloy. *Lab Chip* 8, 1104−1109.

(8) Choi, Y., et al. (2010) A high throughput microelectroporation device to introduce a chimeric antigen receptor to redirect the specificity of human T cells. *Biomed. Microdevices* 12, 855−863.

(9) Gong, X., Yi, X., Xiao, K., Li, S., Kodzius, R., Qin, J., and Wen, W. (2010) Wax-bonding 3D microfluidic chips. *Lab Chip* 10, 2622−2627.

(10) Zhu, T., Luo, C., Huang, J., Xiong, C., Ouyang, Q., and Fang, J. (2010) Electroporation based on hydrodynamic focusing of microfluidics with low dc voltage. *Biomed. Microdevices* 12, 35−40.

(11) Shahini, M., and Yeow, J. T. W. (2013) Cell electroporation by CNT-featured microfluidic chip. *Lab Chip* 13, 2585−2590.

(12) Shahini, M., van Wijngaarden, F., and Yeow, J. T. W. (2013) Fabrication of electro-microfluidic channel for single cell electroporation. *Biomed. Microdevices* 15, 759−766.

(13) Cheng, J., Sheldon, E. L., Wu, L., Uribe, A., Gerrue, L. O., Carrino, J., Heller, M. J., and O'Connell, P. O. (1998) Preparation and hybridization analysis of DNA/RNA from *E. coli* on microfabricated bioelectronic chips. *Nat. Biotechnol.* 16, 541−546.

(14) Lin, Y.-C., Li, M., and Wu, C.-C. (2004) Simulation and experimental demonstration of the electric field assisted electroporation microchip for in vitro gene delivery enhancement. *Lab Chip* 4, 104−108.

(15) He, H., Chang, D. C., and Lee, Y.-K. (2006) Micro pulsed radio-frequency electroporation chips. *Bioelectrochemistry* 68, 89−97.

(16) Huang, K.-S., Lin, Y.-C., Su, C.-C., and Fang, C.-S. (2007) Enhancement of an electroporation system for gene delivery using electrophoresis with a planar electrode. *Lab Chip* 7, 86−92.

(17) Jain, T., and Muthuswamy, J. (2007) Bio-chip for spatially controlled transfection of nucleic acid payloads into cells in a culture. *Lab Chip* 7, 1004−1011.

(18) de la Rosa, C., Tilley, P. A., Fox, J. D., and Kaler, K. V. I. S. (2008) Microfluidic Device for Dielectrophoresis Manipulation and Electrodisruption of Respiratory Pathogen Bordetella pertussis. *IEEE Trans. Biomed. Eng.* 55, 2426−2432.

(19) Bahi, M. M., Tsaloglou, M.-N., Mowlem, M., and Morgan, H. (2011) Electroporation and lysis of marine microalga *Karenia brevis* for RNA extraction and amplification. *J. R. Soc., Interface* 8, 601−608.

(20) Zhan, Y., Wang, J., Bao, N., and Lu, C. (2009) Electroporation of cells in microfluidic droplets. *Anal. Chem.* 81, 2027−2031.

(21) Nakayama, T., Namura, M., Tabata, K. V., Noji, H., and Yokokawa, R. (2009) Sequential processing from cell lysis to protein assay on a chip enabling the optimization of an F1-ATPase single molecule assay condition. *Lab Chip* 9, 3567−3573.

(22) Huang, H., Wei, Z., Huang, Y., Zhao, D., Zheng, L., Cai, T., Wu, M., Wang, W., Ding, X., Zhou, Z., Du, Q., Li, Z., and Liang, Z. (2011) An efficient and high-throughput electroporation microchip applicable for siRNA delivery. *Lab Chip* 11, 163−172.

(23) Xu, Y., Yao, H., Wang, L., Xing, W., and Cheng, J. (2011) The construction of an individually addressable cell array for selective patterning and electroporation. *Lab Chip* 11, 2417−2423.

(24) Geng, T., Bao, N., Sriranganathanw, N., Li, L., and Lu, C. (2012) Genomic DNA extraction from cells by electroporation on an integrated microfluidic platform. *Anal. Chem.* 84, 9632−9639.

(25) Adamo, A., Arione, A., sharei, A., and Jensen, K. F. (2013) Flow-through comb electroporation device for delivery of macromolecules. *Anal. Chem.* 85, 1637−1641.

(26) Jokilaakso, N., Salm, E., Chen, A., Millet, L., Guevara, C. D., Dorvel, B., Reddy, B., Karlstrom, A. E., Chen, Y., Ji, H., Chen, Y., Sooryakumar, R., and Bashir, R. (2013) Ultra-localized single cell electroporation using silicon nanowires. *Lab Chip* 13, 336−339.

(27) Lu, H., Schmidt, M. A., and Jensen, K. F. (2005) A microfluidic electroporation device for cell lysis. *Lab Chip* 5, 23−29.

(28) Lu, K.-Y., Wo, A. M., Lo, Y.-J., Chen, K.-C., Lin, C.-M., and Yang, C.-R. (2006) Three dimensional electrode array for cell lysis via electroporation. *Biosens. Bioelectron.* 22, 568−574.

(29) Chang, W. C., and Sretavan, D. W. (2009) Single cell and neural process experimentation using laterally applied electrical fields between pairs of closely apposed microelectrodes with vertical sidewalls. *Biosens. Bioelectron.* 24, 3600−3607.

(30) Wang, S., Zhang, X., Wang, W., and Lee, L. J. (2009) Semicontinuous Flow Electroporation Chip for High-Throughput Transfection on Mammalian Cells. *Anal. Chem.* 81, 4414−4421.

(31) Dalmay, C., Villemejane, J., Joubert, V., Silve, A., Arnaud-Cormos, D., Français, O., Mir, L. M., Leveque, P., and Le Pioufle, B. (2011) A microfluidic biochip for the nanoporation of living cells. *Biosens. Bioelectron.* 26, 4649−4655.

(32) Homhuan, S., Zhang, B., Sheu, F. S., Bettiol, A. A., and Watt, F. F. (2012) Single-cell electroporation using proton beam fabricated biochips. *Biomed. Microdevices* 14, 533−540.

(33) Shah, D., Steffen, M., and Lilge, L. (2012) Controlled electroporation of the plasma membrane in microfluidic devices for single cell analysis. *Biomicrofluidics* 6, 014111.

(34) Xie, C., Lin, Z., Hanson, L., Cui, Y., and Cui, B. (2012) Intracellular Recording of Action Potentials by Nanopillar Electroporation. *Nat. Nanotechnol.* 7, 185−190.

(35) Wu, M., Zhao, D., Wei, Z., Zhong, W., Yan, H., Wang, X., Liang, Z., and Li, Z. (2013) Method for electric parametric characterization and optimization of electroporation on a chip. *Anal. Chem.* 85, 4483−4491.

(36) Geng, T., Zhan, Y., Wang, H.-Y., Witting, S. R., cornetta, K. G., and Lu, C. (2010) Flow-through electroporation based on constant voltage for large-volume transfection of cells. *J. Controlled Release* 144, 91−100.

(37) Adamo, A., Arione, A., Sharei, A., and Jensen, K. F. (2013) Flow-through Comb Electroporation Device for Delivery of Macromolecules. *Anal. Chem.* 85, 1637−1641.

(38) Longsine-Parker, W., Wang, H., Koo, C., Kim, J., Kim, B., Jayaraman, A., and Han, A. (2013) Microfluidic electro-sonoporation: a multi-modal cell portion methodology through simultaneous application of electric field and ultrasonic wave. *Lab Chip* 13, 2144−2152.

(39) Shih, S. C. C., Goyal, G., Kim, P. W., Koutsoubelis, N., Keasling, J. D., Adams, P. D., Hillson, N. J., and Singh, A. K. (2015) A Versatile Microfluidic Device for Automating Synthetic Biology. *ACS Synth. Biol.* 4, 1151−1164.

(40) Xiao, K., Zhang, M., Chen, S., Wang, L., Chang, D. C., and Wen, W. (2010) Electroporation of micro-droplet encapsulated HeLa cells in oil phase. *Electrophoresis* 31, 3175−3180.

(41) Im, D. J., Jeong, S.-N., Yoo, B. S., Kim, B., Kim, D.-P., Jeong, W.-J., and Kang, I. S. (2015) Digital Microfluidic Approach for Efficient Electroporation with High Productivity: Transgene Expression of Microalgae without Cell Wall Removal. *Anal. Chem.* 87, 6592−6599.

(42) Wang, J., Zhan, Y., Ugaz, V. M., and Lu, C. (2010) Vortex-assisted DNA delivery. *Lab Chip* 10, 2057−2061.

(43) Pollack, M. G., Fair, R. B., and Shenderov, A. D. (2000) Electrowetting-based actuation of liquid droplets for microfluidic applications. *Appl. Phys. Lett.* 77, 1725−1726.

(44) Pollack, M. G., Shenderov, A. D., and Fair, R. B. (2002) Electrowetting-based actuation of droplets for integrated microfluidics. *Lab Chip* 2, 96−101.

(45) Srinivasan, V., Pamula, V. K., and Fair, R. B. (2004) An integrated digital microfluidic lab-on-a-chip for clinical diagnostics on human physiological fluids. *Lab Chip* 4, 310−315.

(46) Fair, R. B. (2007) Digital Microfluidics: is true lab-on-a-chip possible? *Microfluid. Nanofluid.* 3, 245−281.

(47) Wheeler, A. R. (2008) Putting electrowetting to work. *Science* 322, 539−540.

(48) Wheeler, A. R., Moon, H., Kim, C. J., Loo, J. A., and Garrell, R. L. (2004) Electrowetting-based microfluidics for analysis of peptides and proteins by matrix-assisted laser desorption/ionization mass spectrometry. *Anal. Chem.* 76, 4833−4838.

(49) Cho, S. K., Moon, H., and Kim, C. J. (2003) Creating, Transporting, Cutting, and Merging Liquid Droplets by Electrowetting-Based Actuation for Digital Microfluidic Circuits. *J. Microelectromech. Syst.* 12, 70−80.

(50) Lippmann, G. (1875) Relations entre les phénomènes électriques et capillaires. *Annu. Rev. Chim. Phys.* 5, 494.

(51) Berge, B. (1993) Electrocapillarity and wetting of insulator films by water. *C. R. Acad. Sci., Ser. II* 317, 157−163.

(52) Quilliet, C., and Berge, B. (2001) Electrowetting: A recent outbreak. *Curr. Opin. Colloid Interface Sci.* 6, 34−39.

(53) Lin, Y. Y., Evans, R. D., Welch, E., Hsu, B.-N., Madison, A. C., and Fair, R. B. (2010) Low voltage electrowetting-on-dielectric platform using multi-layer insulators. *Sens. Actuators, B 150*, 465−470.

(54) Lin, Y. Y., Welch, E. R. F., and Fair, R. B. (2012) Low voltage picoliter droplet manipulation utilizing electrowetting-on-dielectric platforms. *Sens. Actuators, B 173*, 338−345.

(55) Samiei, E., Tabrizian, M., and Hoorfar, M. (2016) A review of digital microfluidics as portable platforms for lab-on-a-chip applications. *Lab Chip 16*, 2376−2396.

(56) (2016) *Illumina NeoPrep Library Prep System*, http://www.illumina.com/content/dam/illumina-marketing/documents/products/datasheets/neoprep-system-data-sheet-970-2014-004.pdf.

(57) (2016) *ePlex: Sample-to-Answer Multiplex Molecular Diagnostics*, https://www.genmarkdx.com/wp-content/uploads/2016/07/GNMK-IMC-1039-B-ePlex-4-page-Brochure.pdf.

(58) Madison, A. C., Royal, M. W., and Fair, R. B. (2016) Fluid Transport in Partially Shielded Electrowetting on Dielectric Digital Microfluidic Devices. *J. Microelectromech. Syst. 25*, 593−605.

(59) Madison, A. C. (2015) Scalable Genome Engineering in Electrowetting on Dielectric Digital Microfluidic Systems, Ph.D. Thesis, Duke University, Durham, NC.

(60) Kosuri, S., Goodman, D., Cambray, G., Mutalik, V., Gao, Y., Arkin, A., Endy, D., and Church, G. (2013) Composability of regulatory sequences controlling transcription and translation in *Escherichia coli. Proc. Natl. Acad. Sci. U. S. A. 110*, 14024−14029.

(61) Pestka, S. (1974) The Use of Inhibitors in Studies on Protein Synthesis. *Methods Enzymol. 30*, 261−282.

(62) Misumi, M., and Tanaka, N. (1980) Mechanism of Inhibition of Translocation by Kanamycin and Viomycin: A Comparative Study with Fusidic Acid. *Biochem. Biophys. Res. Commun. 92*, 647−654.

(63) Silve, A., Leray, I., Poignard, C., and Mir, L. M. (2016) Impact of external medium conductivity on cell membrane electropermeabilization by microsecond and nanosecond electric pulses. *Sci. Rep. 6*, 19957.

(64) Garcia, P. A., Ge, Z., Kelley, L. E., Holcomb, S. J., and Buie, C. R. (2017) High efficiency hydrodynamic bacterial electrotransformation. *Lab Chip 17*, 490−500.

(65) Sel, D., Cukjati, D., Batiuskaite, D., Slivnik, T., Mir, L. M., and Miklavcic, D. (2005) Sequential finite element model of tissue electropermeabilization. *IEEE Trans. Biomed. Eng. 52*, 816−827.

(66) Garcia, P. A., Davalos, R. V., and Miklavcic, D. (2014) IA Numerical Investigation of the Electric and Thermal Cell Kill Distributions in Electroporation-Based Therapies in Tissue. *PLoS One 9*, e103083.

(67) Canatella, P. J., and Prausnitz, M. R. (2001) Prediction and optimization of gene transfection and drug delivery. *Gene Ther. 8*, 1464−1469.

(68) Dower, W. J., Miller, J. F., and Ragsdale, C. W. (1988) High efficiency transformation of *E. coli* by high voltage electroporation. *Nucleic Acids Res. 16*, 6127−61−45.

(69) Freeman, S. A., Wang, M. A., and Weaver, J. C. (1994) Theory of electroporation of planar bilayer membranes: predictions of the aqueous area, change in capacitance, and pore-pore separation. *Biophys. J. 67*, 42−57.

(70) Smith, K. C., Neu, J. C., and Krassowska, W. (2004) Model of Creation and Evolution of Stable Electropores for DNA Delivery. *Biophys. J. 86*, 2813−2826.

(71) Friedrich, U., Stachowicz, N., Simm, A., Fuhr, G., Lucas, K., and Zimmermann, U. (1998) High efficiency electrotransfection with aluminum electrodes using microsecond controlled pulses. *Bioelectrochem. Bioenerg. 47*, 103−111.

(72) Turjanski, P., Olaiz, N., Maglietti, F., Michinski, S., Suárez, C., Molina, F. V., and Marshall, G. (2011) The Role of pH Fronts in Reversible Electroporation. *PLoS One 6*, e17303.

(73) Li, Y., Wu, M., Zhao, D., Wei, Z., Zhong, W., Wang, X., Liang, Z., and Li, Z. (2016) Electroporation on microchips: the harmful effects of pH changes and scaling down. *Sci. Rep. 5*, 17817.